Phononic Crystal Tunable via Ferroelectric Phase Transition

Chaowei Xu,[1,2,3] Feiyan Cai,[2,4] Shuhong Xie,[1] Fei Li,[2,3] Rong Sun,[5] Xianzhu Fu,[5] Rengen Xiong,[6] Yi Zhang,[6] Hairong Zheng,[2,3,4,*] and Jiangyu Li[3,7,†]

[1]*Key Laboratory of Low Dimensional Materials and Application Technology of Ministry of Education, School of Materials Science and Engineering, Xiangtan University, Xiangtan 411105, China*
[2]*Paul C. Lauterbur Research Center for Biomedical Imaging, Institute of Biomedical and Health Engineering, Shenzhen Institutes of Advanced Technology, Chinese Academy of Sciences, Shenzhen 518055, China*
[3]*Shenzhen Key Laboratory of Nanobiomechanics, Shenzhen Institutes of Advanced Technology, Chinese Academy of Sciences, Shenzhen 518055, China*
[4]*Beijing Center for Mathematics and Information Interdisciplinary Sciences, Beijing 100048, China*
[5]*Center for Advanced Materials, Shenzhen Institutes of Advanced Technology, Chinese Academy of Sciences, Shenzhen 518055, China*
[6]*Ordered Matter Science Research Centre, Southeast University, Nanjing 211189, China*
[7]*Department of Mechanical Engineering, University of Washington, Seattle, Washington, 98195-2600, USA*

(Received 3 April 2015; revised manuscript received 3 May 2015; published 25 September 2015)

Phononic crystals (PCs) consisting of periodic materials with different acoustic properties have potential applications in functional devices. To realize more smart functions, it is desirable to actively control the properties of PCs on demand, ideally within the same fabricated system. Here, we report a tunable PC made of $Ba_{0.7}Sr_{0.3}TiO_3$ (BST) ceramics, wherein a 20-K temperature change near room temperature results in a 20% frequency shift in the transmission spectra induced by a ferroelectric phase transition. The tunability phenomenon is attributed to the structure-induced resonant excitation of A_0 and A_1 Lamb modes that exist intrinsically in the uniform BST plate, while these Lamb modes are sensitive to the elastic properties of the plate and can be modulated by temperature in a BST plate around the Curie temperature. The study finds opportunities for creating tunable PCs and enables smart temperature-tuned devices such as the Lamb wave filter or sensor.

DOI: 10.1103/PhysRevApplied.4.034009

I. INTRODUCTION

Phononic crystals (PCs) consisting of periodic materials with a diverse elastic modulus and mass density have a great advantage in manipulating acoustic wave propagation and energy flow [1,2]. By modulating the geometry and/or the constituent materials of the PCs, many interesting phenomena can be realized, including the band gap, negative refraction, and localized defect modes, which are promising for potential applications in cloaks, isolators, waveguides, sensors, and filters. It is highly desirable to be able to tune the responses of PCs on demand during these applications, without the need to reconfigure the geometry or the constituents of PCs, though large tunability is rather difficult to achieve in practice. To realize more versatile applications of PCs, much of the effort focuses on developing tunable PCs using smart structures [3–7] and materials [8–17], since their properties can be manipulated by external stimuli such as force, electric field, magnetic field, and temperature. For example, the mechanically triggered transformations of phononic band gaps is theoretically demonstrated through applied load [7]. Control of the elastic wave band gaps in two-dimensional piezoelectric periodic structures by using different polarized directions is theoretically studied [8]. Using the plane-wave-expansion method, Yeh theoretically investigates the elastic band structure of a two-dimensional PC made of electrorheological materials and finds that the electric field has a significant effect on the band gaps [9]. Similarly, through theoretical calculations, it is demonstrated that the band structure of PCs made of magnetostrictive materials is tunable by the external magnetic field [10–12]. Taking the magnetoelectroelastic coupling into account, the elastic wave propagation in two-dimensional magnetoelectroelastic PCs is tuned by electric and magnetic fields [13,14]. Tuning and switching the hypersonic phononic properties is realized through phase transitions of crystallization and melting, which can be tuned by temperature [15]. Recently, it was suggested that ferroelectric ceramics are suitable for tunable PCs, since their acoustic velocities are sensitive to the temperature across the Curie temperature (T_C) [18–21].

*Corresponding author.
hr.zheng@siat.ac.cn
†Corresponding author.
jjli@uw.edu

Nevertheless, most of these studies are theoretical in nature and focus on the obvious effects of external stimuli on the band structure of an infinite PC. Few experimental demonstrations of tunable PCs are reported, and the anomalous properties of the passband in a finite structure [18], which are much more interesting, have not been explored.

$Ba_{1-x}Sr_xTiO_3$ is a lead-free perovskite ferroelectric material that has been extensively investigated [22–24], and its T_C can be continuously modified by varying the Ba/Sr ratio. For instance, T_C of $Ba_{0.7}Sr_{0.3}TiO_3$ (BST) is around the room temperature of 298 K [25], across which large variations in material properties are observed due to the ferroelectric phase transition, making it attractive for tunable applications. Here, we report a PC plate made of BST ceramic that is quite effective in exciting a Lamb wave. By taking advantage of the acoustic transmission enhancement induced by a Lamb wave in the PC plate [26,27], thermal tuning of multipeak acoustic transmission through the PC plate is demonstrated with 20% tunability in frequency. The tunability is based on the ferroelectric phase transition of BST that results in a large variation of its acoustic properties across T_C [28], allowing us to tune the transmission of PCs via a temperature-induced ferroelectric phase transition.

II. EXPERIMENT METHODS

The BST ceramic is fabricated by the conventional solid-state reaction technique and followed by the viscous polymer processing route. First, barium carbonate ($BaCO_3$, Aladdin, ≥99%), strontium carbonate ($SrCO_3$, Aladdin, ≥99%), and titania (TiO_2, Aladdin, ≥99%) powders are mixed in the appropriate molar ratios and ground thoroughly by an agate ball grinding mill for 10 h. Second, the mixtures are calcined at 1100°C for 2 h in alumina crucibles opened to air after preloading and then ground for another 10 h. The ground powders are uniformly mixed with an appropriate amount of polyvinyl alcohol (PVA, Sigma) solution (mass concentration 3%) for granulating. Afterwards, the produced mixtures are compressed under the uniaxial pressure of 20 MPa into disks 20 mm in diameter. In order to remove additive polymer, the pelletized disks are first heated up to 600°C at a heating rate of 5°C/ min. The samples are finally sintered at 1400°C for 4 h in alumina crucibles opened to air.

The BST ceramic exhibits a dense grain structure with the grain size ranging from 10 to 30 μm, as seen from the scanning electron microscope (SEM, Nova NanoSEM 450, FEI) images of the surface and cross section in Figs. 1(a) and 1(b). X-ray diffraction (XRD, XD-3A, SHIMADZU) with Cu Kα radiation is used to characterize the phase structures and chemical-component elements. The perovskite phase of the BST with tetragonal space group $P4mm$ is confirmed by the XRD pattern at 293 K, as shown in Fig. 1(c) (black line), with which the lattice parameters are determined to be $a = b = 3.9853$ Å and $c = 3.9541$ Å. Only a slight shift in diffraction peak positions is observed in the XRD pattern measured at 313 K (red line), and the corresponding lattice parameters are determined to be $a = b = c = 3.9754$ Å, suggesting a tetragonal-cubic phase transition. To investigate the phase transition of BST, differential scanning calorimetry (DSC) is undertaken under a nitrogen atmosphere in aluminum crucibles at a heating rate of 5°C/min using a DSC Q20 from TA Instruments, revealing an endothermic effect at the temperature of 303 K [Fig. 1(d)]. To verify that the phase transition is ferroelectric in nature, the temperature dependence of the dielectric constant of BST is measured by using a high-precision LCR meter (4282a, Agilent) at 500 Hz–1 MHz from −160 to 160°C [Fig. 1(e)], exhibiting three peaks at around 176, 225, and 298 K, corresponding to consecutive rhombohedral-orthorhombic-tetragonal-cubic phase transitions that are well documented in the literature [24,25]. An increase in the dielectric dispersion with frequency can be observed in the BST ceramic, indicating that BST has a diffuse phase transition owing to the substitution of Sr on the Ba site [26]. The polarization-electric field hysteresis loops of BST ceramic are recorded on a Sawyer-Tower circuit (Precision Premier II, Radiant Technologies, Inc.) at different temperatures, revealing typical ferroelectric hysteresis at lower temperatures [Fig. 1(f)]. The hysteresis loop gradually decreases with the increased temperature and diminishes at 330 K, further confirming the ferroelectric phase transition of BST.

III. SIMULATION AND EXPERIMENT RESULTS

Across the ferroelectric phase transition, large variations of material properties are expected, as exhibited by the dielectric constant and ferroelectric hysteresis. Particularly relevant to our study are the acoustic velocities in BST ceramic, which are measured by ultrasonic techniques, using the conventional pulse-echo technique with longitudinal and transversal ultrasonic waves. As shown in Fig. 2(a), the acoustic velocities are a function of temperature for longitudinal (c_l, square solid dots) and transverse (c_t, square solid dots) wave velocities in BST. A large increase in acoustic velocities occurs when the temperature changes from 293 to 313 K, and outside of this range they are relatively stable, consistent with the tetragonal-cubic phase transition of BST in this temperature range. The specific wave velocities of BST are measured to be $c_l = 5340$ m/s and $c_t = 3345$ m/s for 293 K and $c_l = 6163$ m/s and $c_t = 4161$ m/s for 313 K, respectively. The density of BST, 5400 kg/m^3 as measured by the Archimedean method, is almost constant in the temperature range from 293 to 313 K.

Furthermore, the dispersion curves of a uniform BST plate with thickness $t = 0.5$ mm immersed in water are calculated at temperatures 293 and 313 K, respectively, as shown in Fig. 2(b), where A_n and S_n represent antisymmetric and symmetric Lamb modes, respectively, and n $(0, 1, \ldots)$

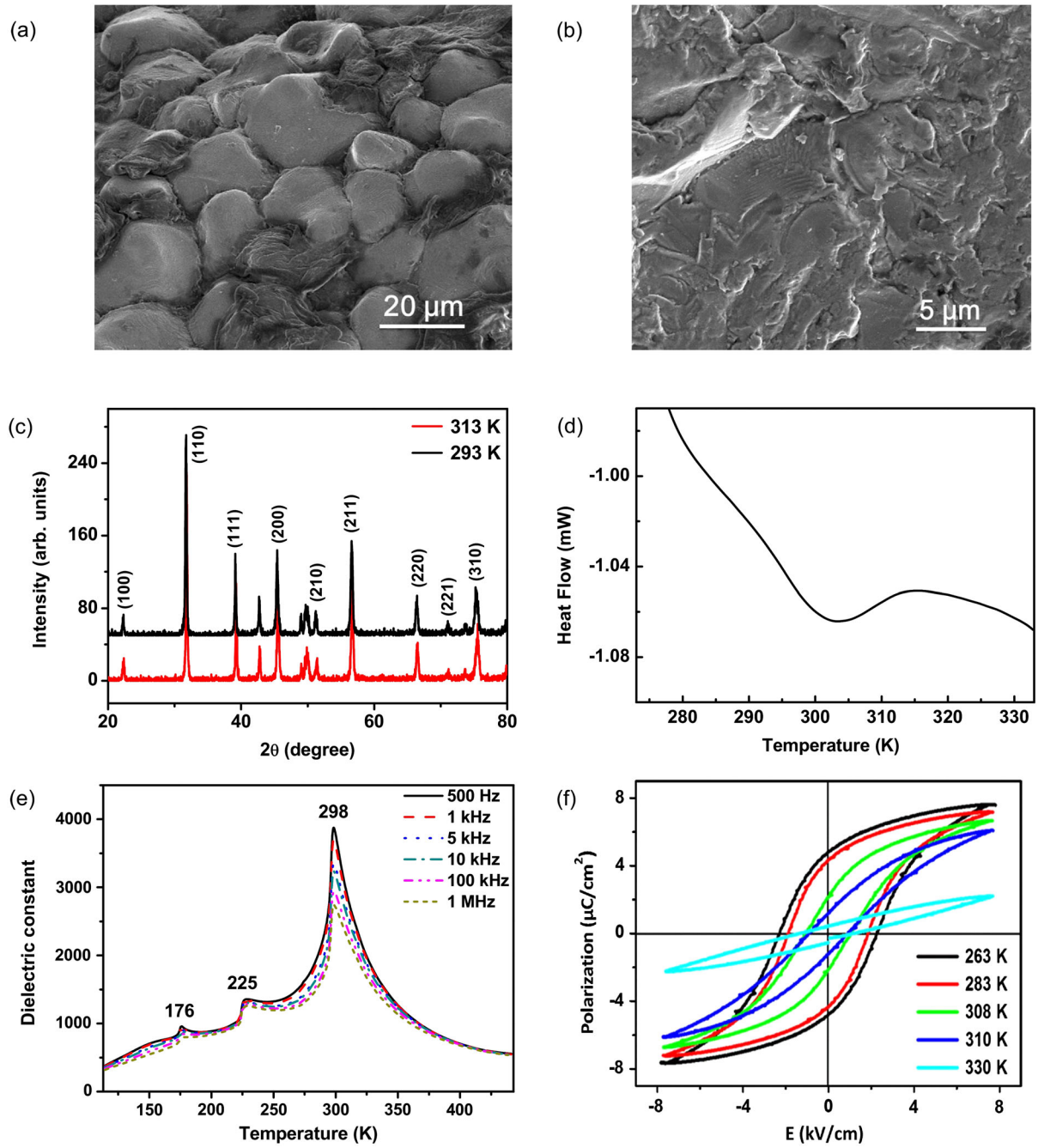

FIG. 1. Ferroelectric phase transition of BST. (a) Surface SEM micrographs of BST ceramic. (b) Cross-section SEM micrographs. (c) XRD patterns at temperature of 293 and 313 K. (d) DSC curve. (e) The variation in the dielectric constant as a function of temperature at the frequency from 500 Hz to 1 MHz. (f) Ferroelectric hysteresis loops at temperatures above and below T_C.

characterizes their orders. They clear demonstrate Lamb modes in a BST plate, which originate from the coupling of longitudinal and transverse waves via reflection from the finite boundary [29,30] and are sensitive to the temperature. It is worth noting that the higher the frequency is, the more sensitive A_0 and S_0 modes are to the temperature, while there are more high-order modes. Thus, at low frequency it would be difficult to sensor a mode using a different temperature, since the mode shifts for a different temperature are not obvious. At a high frequency, it is also difficult to sensor a pure mode, as many high modes are generated. At an intermediate frequency, if few of these low-order Lamb modes can be excited, then the BST can be used as an efficient temperature-tuned Lamb wave filter or sensor.

In order to excite and modulate a Lamb mode in BST, we design and fabricate a one-dimensional PC plate model (thickness $t = 0.5$ mm) that has one side patterned with a periodical array (period $p = 1.0$ mm) of rectangular

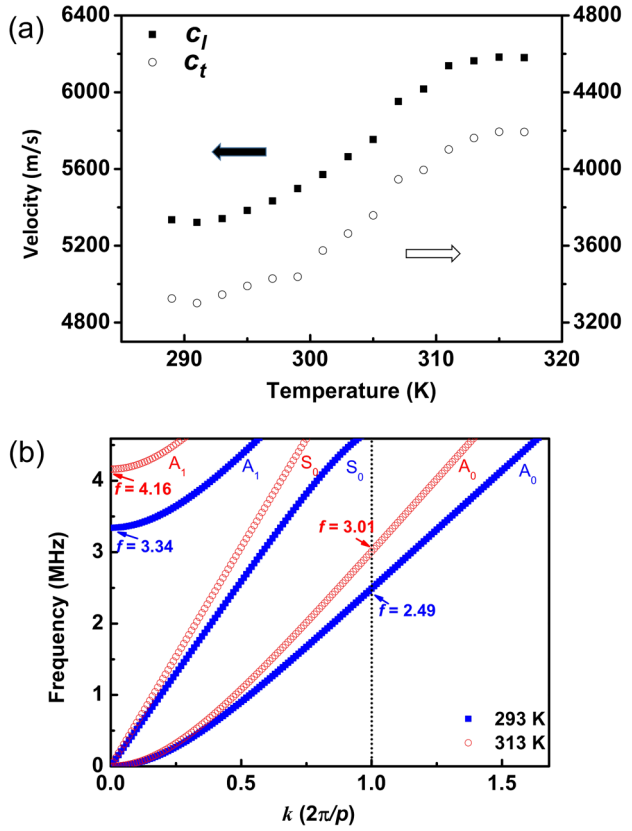

FIG. 2. (a) Longitudinal and transverse wave velocities measured at temperatures ranging from 289 to 317 K. (b) Dispersion curves of a Lamb wave in a uniform BST ceramic of thickness $t = 0.5$ mm immersed in water at 293 (blue square dots) and 313 K (red circle dots).

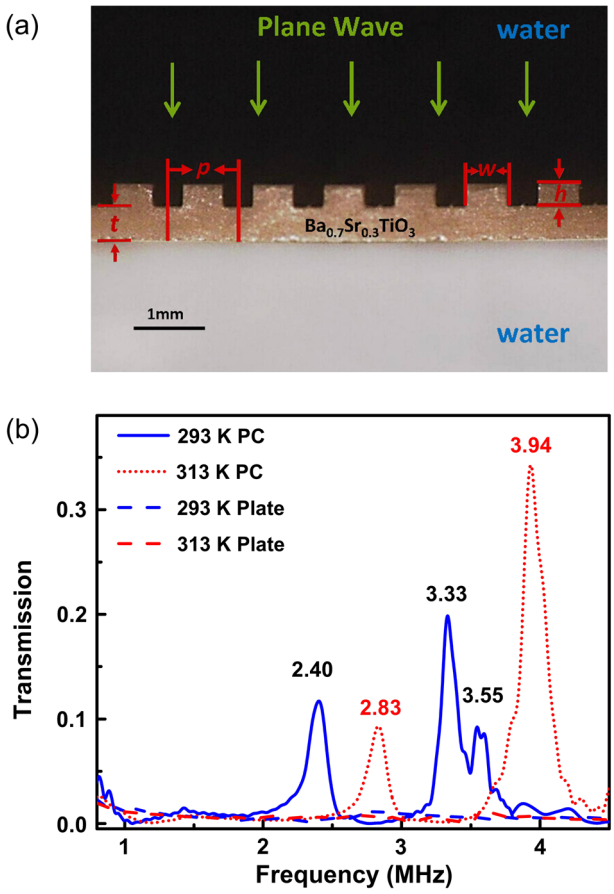

FIG. 3. (a) Schematic representation and photograph of the PC plate. (b) The experimental power-transmission coefficients of PCs (solid line and dotted line) and a uniform BST plate (dashed line) at 293 (blue) and 313 K (red).

gratings (width $w = 0.6$ mm and height $h = 0.3$ mm), as shown in Fig. 3(a). Under the normal incidence of a plane acoustic wave from the structured side, the power-transmission coefficients of a BST PC plate are measured in water at temperatures 293 (blue solid line) and 313 K (red dotted line) and compared to those of a uniform BST plate (dashed line), shown in Fig. 3(b). The transmitted signals are generated and received by a computer-controlled pulse receiver (5800PR, Olympus) and digitized at a sampling frequency of 100 Msa/s (Octopus 822F, GAGE, Lockport, IL, USA). It is evident that the transmission for the uniform reference plate is rather low in the considered frequency range and is insensitive to the temperature change, in spite of the large difference in wave velocities. This is because of the mismatch of momentum between A_0 and S_0 modes with water, as well as the mismatch of symmetry of the A_1 mode with respect to the source [31]. These Lamb modes in a uniform BST plate cannot be excited by normal incidence [32,33]. On the other hand, the spectra of a BST PC show large transmission enhancement peaks at 2.40, 3.33, and 3.55 MHz at 293 K, which change to 2.83 and 3.94 MHz at 313 K. This set of experiment results thus demonstrates that the designed PC structure is necessary to excite the Lamb waves in BST [26,27], and such Lamb waves can be tuned by the temperature change.

To further investigate the tunable transmission peaks, by using a finite-element analysis and solver software package of COMSOL Multiphysics [34], the transmission spectra of a BST PC plate and a uniform BST plate are simulated at 293 and 313 K, respectively, as shown in Fig. 4(a). These frequencies of transmission peaks agree well with the experimental spectra of Fig. 3(b), even though there is a size deviation between the experiment sample and the designed sample. It is clearly observed that the first remarkable peak at a frequency of 2.47 MHz shifts to a frequency of 2.93 MHz when the temperature is changed from 293 to 313 K, corresponding to an 18.6% frequency tenability over a 20-K temperature range. Similarly, the second peak of 3.35 MHz at 293 K changes to 4.07 MHz at 313 K, a frequency shift of 21.5%. The transmission spectra as a continuous function of temperature are simulated and shown in Fig. 4(b), which makes the trend of thermal tuning more visual. As expected, the frequency trends of transmission peaks fit into the change of acoustic

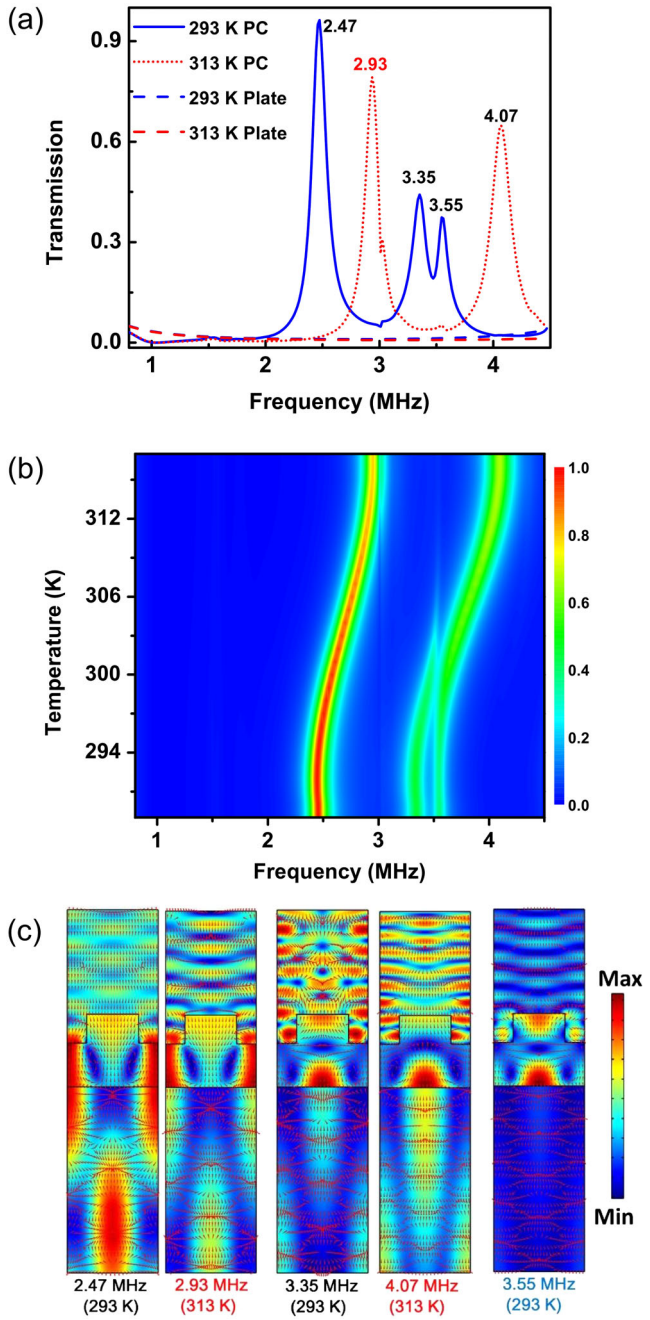

FIG. 4. (a) The simulated power-transmission coefficients of BST PCs (solid line and dot line) and a uniform BST plate (dashed line) at 293 (blue) and 313 K (red). (b) Transmission spectra of BST PCs as a function of temperature from 289 to 317 K. (c) The simulated velocity field distribution of one unit cell of a BST PC at 2.47, 3.35, and 3.55 MHz at 293 K and 2.93 and 4.07 MHz at 313 K; both the amplitude field (color variations) and the vector field (arrows) are provided.

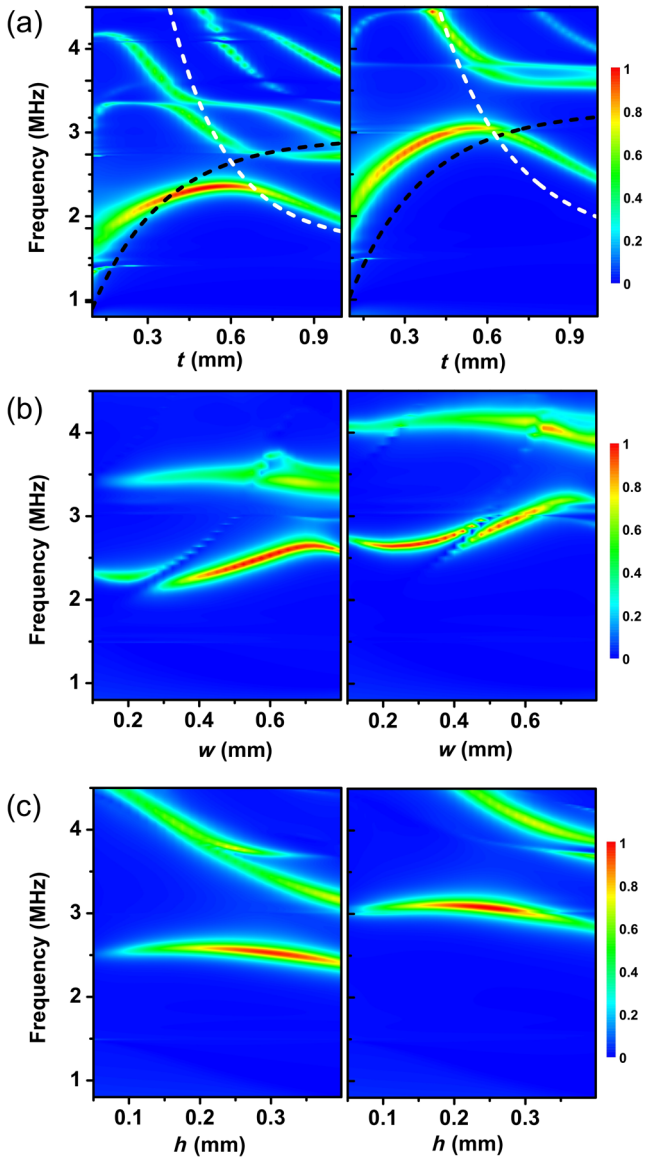

FIG. 5. Transmission spectra versus geometric parameters [thickness t of a BST substrate (a), width w (b), and height h (c) of gratings] at 293 (left) and 313 K (right) for a series of BST PC samples with other geometric parameters identical to the aforementioned. In (a), the dark dashed line and the white dashed line give a theoretical prediction of the frequency of the A_0 mode at $k = 2\pi/p$ and the A_1 mode at $k = 0$ in the uniform brass plate of thickness t, respectively.

velocities with temperature. In addition, these velocity field distributions of five transmission enhancement peaks in Fig. 4(a) are shown in Fig. 4(c).

By comparing the velocity field distribution of each peak at these two temperatures, it is revealed that the excited modes of 2.47 MHz at 293 K and 2.93 MHz at 313 K are the same; so are the excited modes of 3.35 MHz at 293 K and 4.07 MHz at 313 K. The third peak of 3.55 MHz at 293 K in both the experiment and the simulation does not appear at 313 K. As shown in the last field distribution in Fig. 4(c), this peak originates from the coupling of resonance of water between gratings and the Lamb mode in a BST PC. Furthermore, comparing Fig. 4(a) with Fig. 2(b), these frequencies of the first peak at 293 and 313 K almost coincide with these frequencies of the A_0

mode at $k = 2\pi/p$ in a uniform BST plate, while these frequencies of the second peak at 293 and 313 K are almost the same with these frequencies of the A_1 mode at $k = 0$ in a uniform BST plate. It can be explained that the Bragg scattering by the gratings on the BST PC, which folds the A_0 mode at $k = 2\pi/p$ back to $k = 0$ as well as changes the symmetry of the A_1 mode, leads to these two modes matching momentum and symmetry with respect to the normal incident source [26,27]. Thus, the first and second peaks at both 293 and 313 K originate from the resonant excitation of the A_0 and A_1 modes that exist intrinsically in the uniform elastic plate, respectively, while these Lamb modes can be effectively modulated around T_C.

In order to investigate the geometrical parameters of BST PC influence on the existence and trend of the resonant peaks, Fig. 5 shows the transmission spectra for temperatures 293 and 313 K varying with the thickness t of the substrate and width w and height h of gratings, respectively, for a series of BST PC samples with other geometrical parameters identically to the aforementioned. In Fig. 5(a), the dark dashed line and the white dashed line give a theoretical prediction of the frequency of the A_0 mode at $k = 2\pi/p$ and the A_1 mode at $k = 0$ in the uniform brass plate of thickness t, respectively. As shown in Fig. 5(a), for a small value of t, the difference of the first transmission peak in the two temperatures is not distinct, which is due to the corresponding A_0 mode in the thin plate shifting for different temperatures not being obvious. For an intermediate value of t, as mentioned earlier, these positions of the first and the second transmission peak for both temperatures agree well with these predicted from the A_0 mode at $k = 2\pi/p$ and the A_1 mode at $k = 0$ in the uniform plate, respectively. For a large value of t, multiple transmission peaks are arising and cannot be distinguished effectively in the two temperatures, which is due to high-order Lamb modes arising in the thick plate. Therefore, it is reasonable to choose an intermediate value of thickness t as 0.5 mm for the sample of BST PC substrate in the experiment.

In Fig. 5(b), it is clearly shown that the width w of grating influences the frequency and shape of the first transmission peak. As shown in Fig. 5(c), the height h of the gratings affects the frequency and shape of the second transmission peak. These phenomena can be explained from the characteristic of the displacement field for the A_0 and A_1 Lamb modes in a uniform plate [35]. For the A_0 mode at $k = 2\pi/p$, the longitudinal component of displacement is maximized at the surface of plate, while the transverse component is almost invariant across the plate thickness; thus, the displacement of this mode is sensitive to the longitudinal displacement component. The A_1 mode at $k = 0$ in the uniform plate is the cutoff mode, while the product of frequency multiplied by the plate thickness is equal to half the transverse wave velocity; thus, the displacement of this mode is pure transverse. For Lamb waves in an isotropic plate, the longitudinal displacement is parallel to the surface, while the transverse displacement is normal to the surface. Thus, the A_0 mode at $k = 2\pi/p$ is more sensitive to the perturbation of BST PCs on the direction parallel to the surface, i.e., the width of a grating on a BST substrate. The A_1 mode at $k = 0$ is more sensitive to the perturbation of BST PCs on the direction normal to the surface, i.e., the height of a grating on a BST substrate. Accordingly, the first and the second transmission peaks originate from the structure-induced resonant excitation of A_0 and A_1 Lamb modes that exist intrinsically in the uniform BST plate, which are sensitive to the width w and the height h of gratings, respectively. After considering the trends of w and h influence on these two peaks in two temperatures, it is reasonable to choose the width as 0.6 mm and the height as 0.3 mm for the grating on the surface of BST PCs in the experiment.

IV. CONCLUSION

In conclusion, we fabricate ferroelectric ceramic materials BST with the phase transition temperature T_C at room temperature, across which the acoustical properties show substantial variation. PCs consisting of periodic artificial structure on the surface of a BST plate are found to be suitable for multifrequency transmission enhancement, where transmission peaks show large thermal tunability around 20% over a 20-K temperature range near room temperature. The phenomenon is attributed to the structured-induced resonant excitation of A_0 and A_1 Lamb modes that exist intrinsically in the uniform elastic plate, while these Lamb modes are sensitive to the elastic properties (longitudinal and transverse wave velocities) of the plate and can be modulated by the temperature in a BST plate around T_C. The tunable PC via a ferroelectric phase transition will pave the way to explore acoustic properties of ferroelectric materials and has promising prospects for tunable smart devices, such as a temperature-tuned Lamb wave filter or sensor.

ACKNOWLEDGMENTS

The work is partially supported by National Natural Science Foundation of China (Grants No. 11274008, No. 11325420, and No. 11404363) and National 973 Program (Grant No. 2015CB755500) and is carried out at Shenzhen Key Laboratory of Nanobiomechanics. F. C. acknowledges partial support by Shenzhen Key Laboratory for Molecular Imaging. F. L. acknowledges partial support by China Postdoctoral Science Foundation 2014M560682. C. X. and S. X. acknowledge partial support by National Natural Science Foundation of China (Grant No. 11372268) and Provincial Natural Science Foundation of Hunan, China (Grant No. 13JJ1019). J. L. acknowledges support by NSF (CMMI-1100339).

C. X. and F. C. contributed equally to this work.

[1] M. Kushwaha, P. Halevi, G. Martinez, L. Dobrzynski, and B. Djafari-Rouhani, Theory of acoustic band structure of periodic elastic composites, Phys. Rev. B **49**, 2313 (1994).

[2] Y. Pennec, J. O. Vasseur, B. Djafari-Rouhani, L. Dobrzyński, and P. A. Deymier, Two-dimensional phononic crystals: Examples and applications, Surf. Sci. Rep. **65**, 229 (2010).

[3] D. Caballero, J. Sanchez-Dehesa, C. Rubio, R. Martinez-Sala, J. Sanchez-Perez, F. Meseguer, and J. Llinares, Large two-dimensional sonic band gaps, Phys. Rev. E **60**, R6316 (1999).

[4] X. Zhou, Y. Wang, and C. Zhang, Effects of material parameters on elastic band gaps of two-dimensional solid phononic crystals, J. Appl. Phys. **106**, 014903 (2009).

[5] A. Khelif, P. Deymier, B. Djafari-Rouhani, J. Vasseur, and L. Dobrzynski, Two-dimensional phononic crystal with tunable narrow pass band: Application to a waveguide with selective frequency, J. Appl. Phys. **94**, 1308 (2003).

[6] Y. Pennec, B. Djafari-Rouhani, J. Vasseur, A. Khelif, and P. Deymier, Tunable filtering and demultiplexing in phononic crystals with hollow cylinders, Phys. Rev. E **69**, 046608 (2004).

[7] K. Bertoldi and M. Boyce, Mechanically triggered transformations of phononic band gaps in periodic elastomeric structures, Phys. Rev. B **77**, 052105 (2008).

[8] X. Y. Zou, Q. Chen, B. Liang, and J. C. Cheng, Control of the elastic wave bandgaps in two-dimensional piezoelectric periodic structures, Smart Mater. Struct. **17**, 015008 (2008).

[9] J. Y. Yeh, Control analysis of the tunable phononic crystal with electrorheological material, Physica (Amsterdam) **400B**, 137 (2007).

[10] J. F. Robillard, O. B. Matar, J. Vasseur, P. Deymier, M. Stippinger, A. C. Hladky-Hennion, Y. Pennec, and B. Djafari-Rouhani, Tunable magnetoelastic phononic crystals, Appl. Phys. Lett. **95**, 124104 (2009).

[11] J. Vasseur, O. B. Matar, J. F. Robillard, A. C. Hladky-Hennion, and P. Deymier, Band structures tunability of bulk 2D phononic crystals made of magneto-elastic materials, AIP Adv. **1**, 041904 (2011).

[12] Z. Xu, F. Wu, and Z. Guo, Shear-wave band gaps tuned in two-dimensional phononic crystals with magnetorheological material, Solid State Commun. **154**, 43 (2013).

[13] Y. Wang, F. Li, K. Kishimoto, Y. Wang, and W. Huang, Elastic wave band gaps in magnetoelectroelastic phononic crystals, Wave Motion **46**, 47 (2009).

[14] Y. Wang, F. Li, W. Huang, X. Jiang, Y. Wang, and K. Kishimoto, Wave band gaps in two-dimensional piezoelectric/piezomagnetic phononic crystals, Int. J. Solids Struct. **45**, 4203 (2008).

[15] A. Sato, Y. Pennec, N. Shingne, T. Thurn-Albrecht, W. Knoll, M. Steinhart, B. Djafari-Rouhani, and G. Fytas, Tuning and switching the hypersonic phononic properties of elastic impedance contrast nanocomposites, ACS Nano **4**, 3471 (2010).

[16] W. Cheng, J. Wang, U. Jonas, G. Fytas, and N. Stefanou, Observation and tuning of hypersonic bandgaps in colloidal crystals, Nat. Mater. **5**, 830 (2006).

[17] H. Tang, C. Luo, and X. Zhao, Tunable characteristics of a flexible thin electrorheological layer for low frequency acoustic waves, J. Phys. D **37**, 2331 (2004).

[18] K. Jim, C. Leung, S. Lau, S. Choy, and H. Chan, Thermal tuning of phononic bandstructure in ferroelectric ceramic/epoxy phononic crystal, Appl. Phys. Lett. **94**, 193501 (2009).

[19] Y. Yao, F. Wu, X. Zhang, and Z. Hou, Thermal tuning of Lamb wave band structure in a two-dimensional phononic crystal plate, J. Appl. Phys. **110**, 123503 (2011).

[20] Y. Cheng, X. Liu, and D. Wu, Band structures of phononic-crystal plates in the form of a sandwich-layered structure, J. Acoust. Soc. Am. **130**, 2738 (2011).

[21] Z. Bian, W. Peng, and J. Song, Thermal tuning of band structures in a one-dimensional phononic crystal, J. Appl. Mech. **81**, 041008 (2014).

[22] C. Fu, C. Yang, H. Chen, Y. Wang, and L. Hu, Microstructure and dielectric properties of $Ba_xSr_{1-x}TiO_3$ ceramics, Mater. Sci. Eng. B **119**, 185 (2005).

[23] O. Thakur, C. Prakash, and D. Agrawal, Dielectric behavior of $Ba_{0.95}Sr_{0.05}TiO_3$ ceramics sintered by microwave, Mater. Sci. Eng. B **96**, 221 (2002).

[24] L. Benguigui, Disordered ferroelectrics: $Ba_xSr_{1-x}TiO_3$ single crystals, Phys. Status Solidi A **46**, 337 (1978).

[25] K. Bethe and F. Welz, Preparation and properties of (Ba, Sr) TiO_3 single crystals, Mater. Res. Bull. **6**, 209 (1971).

[26] Z. He, H. Jia, C. Qiu, S. Peng, X. Mei, F. Cai, P. Peng, M. Ke, and Z. Liu, Acoustic Transmission Enhancement through a Periodically Structured Stiff Plate without Any Opening, Phys. Rev. Lett. **105**, 074301 (2010).

[27] H. Jia, M. Ke, C. Li, C. Qiu, and Z. Liu, Unidirectional transmission of acoustic waves based on asymmetric excitation of Lamb waves, Appl. Phys. Lett. **102**, 153508 (2013).

[28] A. Moreno-Gobbi, D. Garcia, J. A. Eiras, and A. S. Bhalla, Study by ultrasonic techniques of the phase diagram of BST ceramic family mainly for high Sr concentrations, Ferroelectrics **337**, 197 (2006).

[29] H. Lamb, On waves in an elastic plate, Proc. R. Soc. A **93**, 114 (1917).

[30] J. Wu and Z. Zhu, The propagation of Lamb waves in a plate bordered with layers of a liquid, J. Acoust. Soc. Am. **91**, 861 (1992).

[31] F. L. Hsiao, A. Khelif, H. Moubchir, A. Choujaa, C. C. Chen, and V. Laude, Complete band gaps and deaf bands of triangular and honeycomb water-steel phononic crystals, J. Appl. Phys. **101**, 044903 (2007).

[32] M. Castaings and P. Cawley, The generation, propagation, and detection of Lamb waves in plates using air-coupled ultrasonic transducers, J. Acoust. Soc. Am. **100**, 3070 (1996).

[33] V. Dayal and V. K. Kinra, Leaky Lamb waves in an anisotropic plate. I: An exact solution and experiments., J. Acoust. Soc. Am. **85**, 2268 (1989).

[34] http://www.comsol.com/.

[35] R. Daniel and D. Eugene, *Elastic Waves in Solids I: Free and Guided Propagation* (Springer, New York, 2000), p. 318.